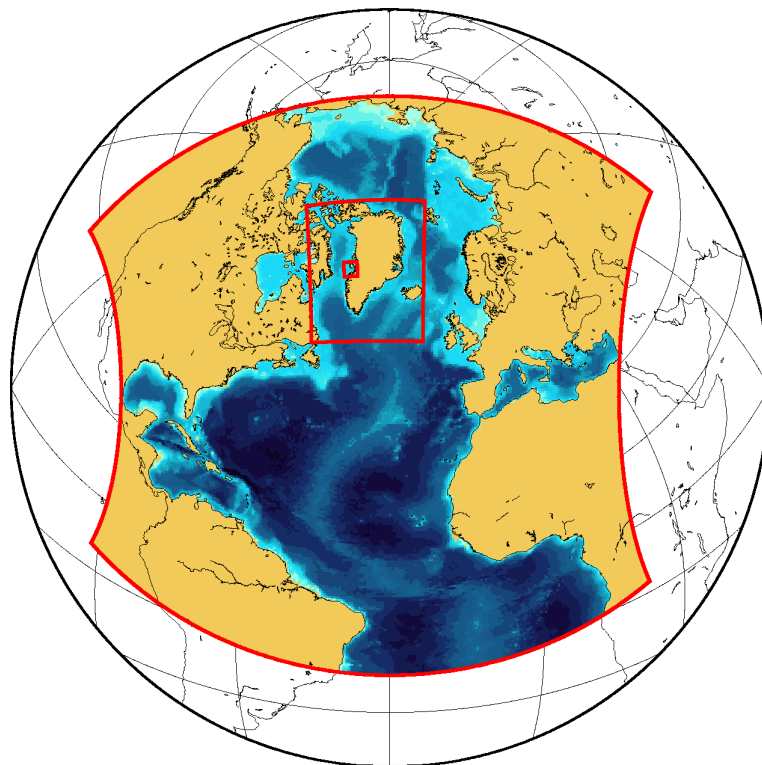**DMi**
Ministry of Transport and Energy

Technical Report 06-07

HYCOM for the North Atlantic Ocean with special emphasis on West Greenland Waters

Mads Hvid Ribergaard, Nicolai Kliem and Martin Jespersen

Copenhagen 2006

Colophon

Content:

Abstract

A one-year simulation of the Greenland Waters for the period July 1 2004 to July 1 2005 is performed with the three-dimensional hydrodynamic ocean model HYCOM. The resolution is 10km, with a high resolution (2km) domain for the Disko Bay.

Resumé

En et-års simulering af de grønlandske farvande for perioden fra d. 1. juni 2004 til d. 1. juni 2005 er foretaget med den 3-dimensionelle hydrodynamiske model HYCOM. Opløsningen er 10km, med højere opløsning (2km) for et underområde dækkende Diskobugten.

1. Introduction

This report deals with hydrodynamic simulations in the region between West Greenland and Baffin Island, focusing on the shelf region off Disko Island and Disko Bay. The calculations are done with a three-dimensional ocean model which simulates the physical processes in the ocean. Prerequisites for the ocean model are detailed knowledge of the surface wind as obtained from the operational numerical weather prediction model HIRLAM. Initial and boundary hydrographic values are obtained from the World Ocean Atlas.

The model is set up in a nested version with one grid covering the entire North Atlantic and Arctic Ocean simulating the overall current system and providing boundary conditions for a higher resolution domain covering the waters around Greenland. A third nesting level with even higher resolution is applied for the Disko Bay area. The simulation is applied for the design year mid-2004 to mid-2005, initialized mid-2003 with a one year spin-up period.

The report is organized as follows. In Chapter 2 a general description of the oceanographic conditions off West Greenland is given. The numerical modelling is described in Chapter 3 while a few examples of model results are shown in Chapter 4.

The work has been funded by the Danish National Environmental Research Institute (NERI) as part of the cooperation between NERI and the Bureau of Minerals and Petroleum, Greenland Home Rule, on developing a Strategic Environmental Impact Assessment of oil exploration activities in the Southeastern Baffin Bay.

2. Oceanographic conditions off West Greenland

The ocean currents around Greenland are part of the cyclonic subpolar gyre circulation of the North Atlantic and the Arctic region. The bottom topography plays an important role for guiding the circulation and for the distributing the water masses (compare Figure 1 and Figure 2).

Bottom topography

The northern part of the Atlantic Ocean consists of the Labrador Basin, the Irminger Basin and the Iceland Basin which all are semi-closed basins which gradually increase their depth in the southward direction. The ridge between Greenland and Scotland separates the North Atlantic from the Nordic Seas. The two most important routes of the overflow of dense water are the Denmark Strait with a sill depth of about 630 m and the 840 m deep Faroe Bank Channel. The maximum depth between Iceland and Faroe is about 480 m and the Wyville-Thomson Ridge west of Scotland is about 600 m deep. The Nordic Seas consists of three major basins: the Greenland, and Norwegian Basins and the Iceland Plateau. The Nordic Seas are connected to the Arctic Ocean through Fram Strait which is the primary opening and has a depth of more than 2600 m deep. In the Barents Sea another but shallow passage exists.
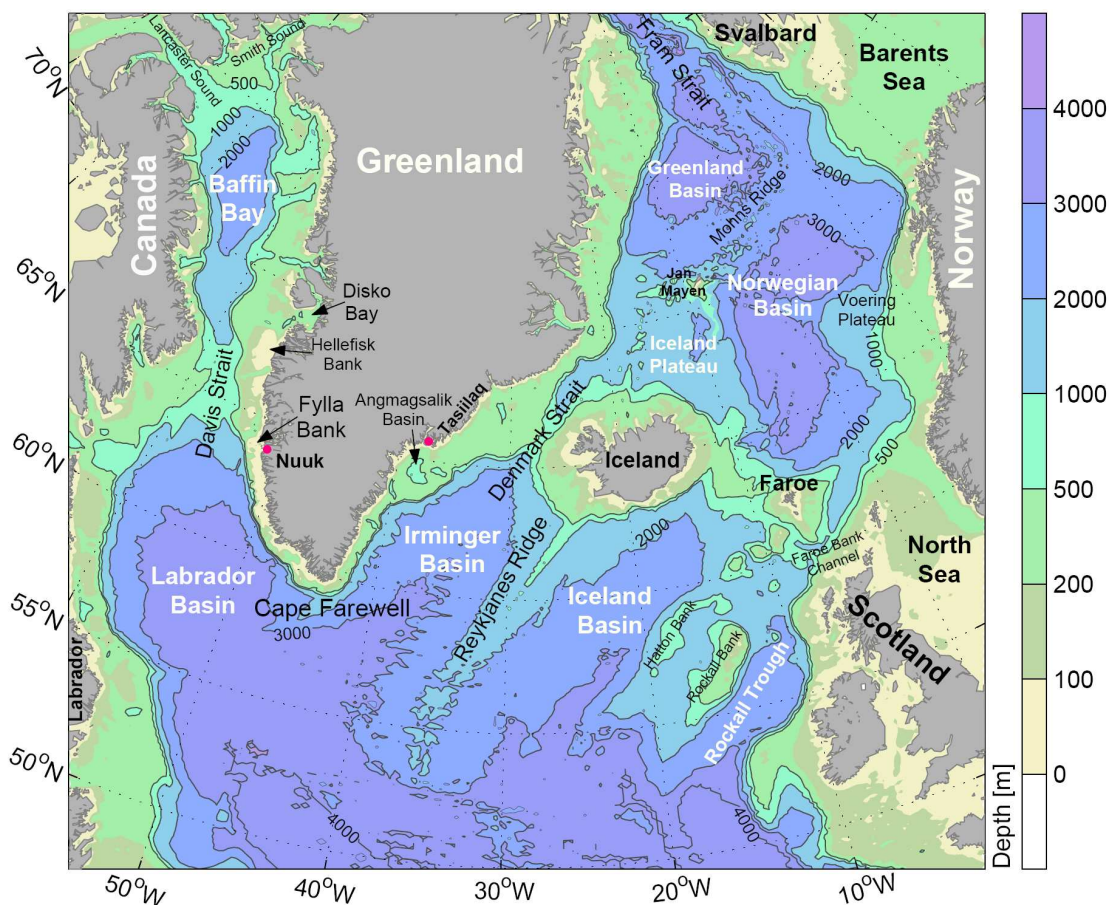
Figure 1. Bottom topography of the North Atlantic including the Nordic Seas. Bottom topography contours at 500, 1000, 2000, 3000 and 4000 m are shown as lines. From Ribergaard (2004).

West of Greenland the Davis Strait makes a 670 m deep opening between the Labrador Basin and Baffin Bay. In the northern part of Baffin Bay the Canadian Archipelago makes a connection to the Arctic Ocean. The primary openings are Smith Sound and Lancaster Sound with depths of a few

hundreds of meters.

Greenland is surrounded by a continental shelf with several banks separated by deep channels formed during the last ice age. The East Greenland shelf is generally wider and deeper than the Southwest Greenland shelf.
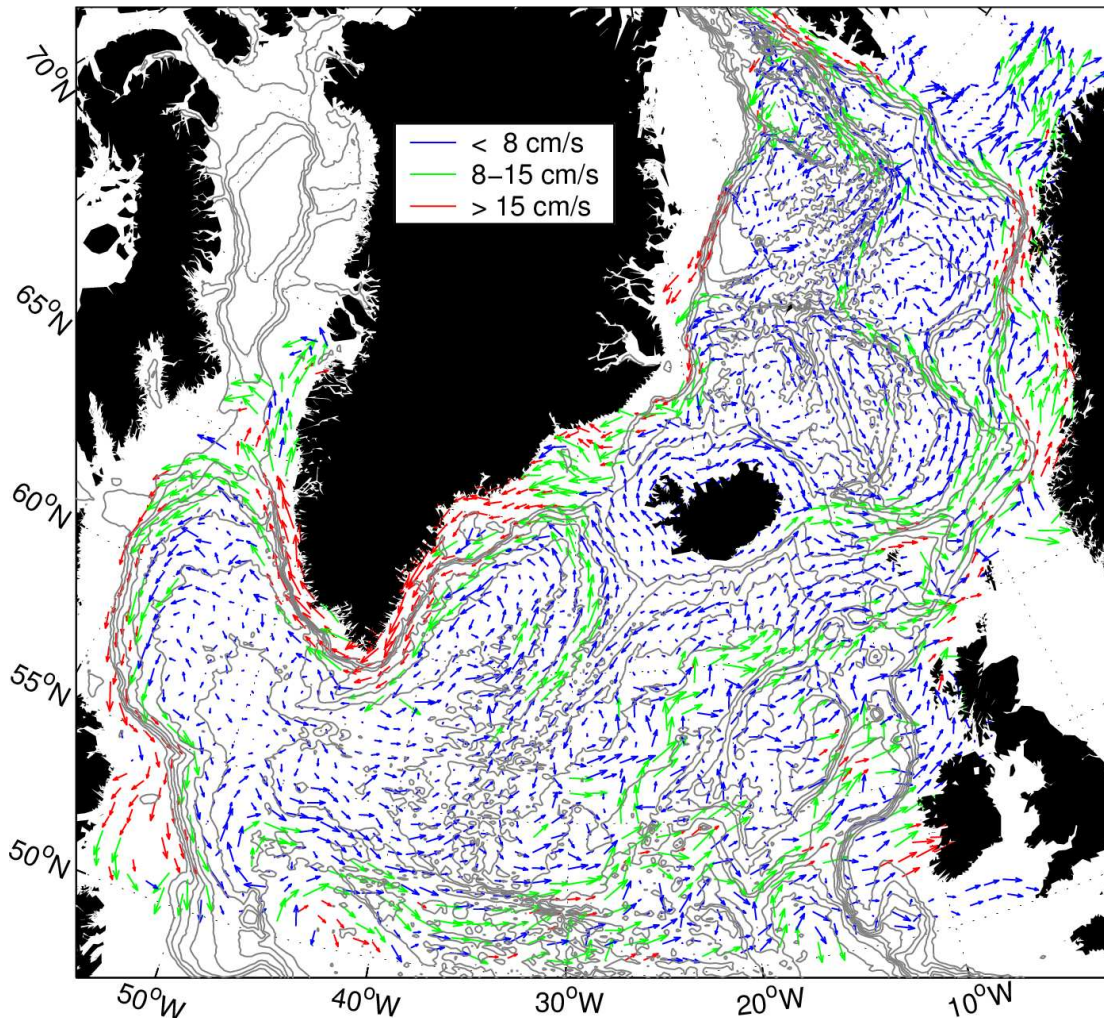

Figure 2. Quasi-Eulerian current vectors at 15 m depth derived from 18 day low-passed filtered drifter trajectories and averaged in overlapping 1° latitude × 2° longitude boxes. Note the different scales for low-velocity (blue), medium-velocity (green) and high-velocity currents (red arrows). Bottom topography at 500 m intervals is shown as grey lines. Reproduced after Jakobsen et al. (2003).

Hydrographic conditions off Southwest Greenland

The surface waters around West Greenland and the Southeast Greenland are primarily composed of two very different water masses:

- Warm and saline Irminger Water (IW), a side branch of the North Atlantic Current.
- Cold and low-saline Polar Water (PW) originating from the Arctic Ocean.

These watermasses meet in the northern Irminger Basin and in Denmark Strait as seen in Figure 3. Here the main branch of the Irminger Current turns west towards East Greenland where it meets the PW, which is transported southward along East Greenland within the East Greenland Current (EGC) (Figure 2). It is the strength of these two currents that determines the hydrographic conditions around Southeast and West Greenland. In the Irminger Basin the two water masses flow

side by side forming large meanders at the front where mixing takes place. PW is found at the surface on the continental shelf whereas IW is found over the continental slope and partly below the PW on the deeper parts of the continental shelf (Figure 4c).
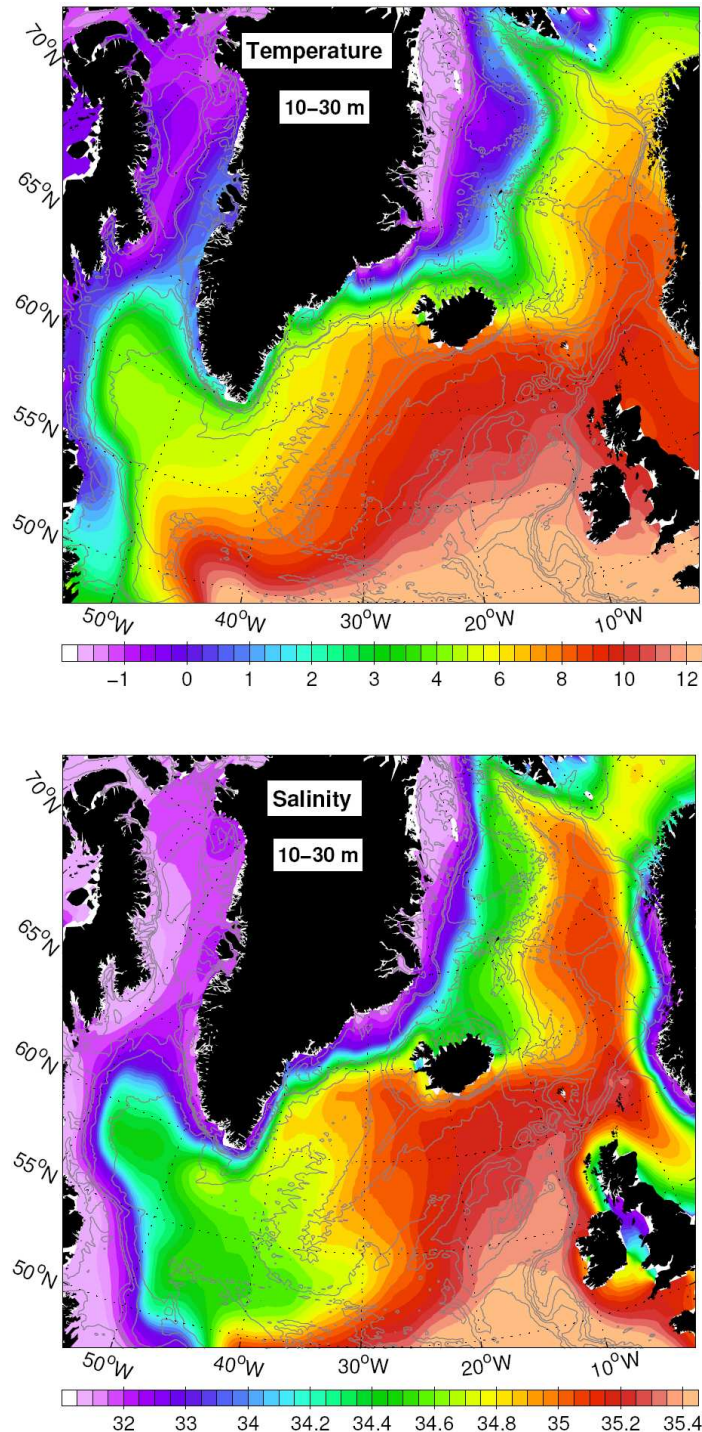
Figure 3. Annual mean surface (10–30 m) temperature (top) and salinity (bottom) from World Ocean Atlas 2001 (WOA2001). Note the change in scales at 4°C for temperature and 34 for salinity. Bottom contours at 500, 1000, 2000, 3000 and 4000 m are shown.

As they round Cape Farewell the IW subducts under the PW (Figure 4b) forming the West Greenland Current (WGC). These watermasses gradually mix along West Greenland, but IW can be traced all along the coast up to the northern parts of Baffin Bay (Buch, 1990). At Cape Farewell IW is found as a 500–800 m thick layer on the continental slope with a core at about 200–300 m. The

depth of the core gradually decreases from east to west (cross-section) as seen in Figure 4b. From south towards north (along-section), the depth of the core gradually increase to below 400 m in the northern Davis Strait and Baffin Bay.
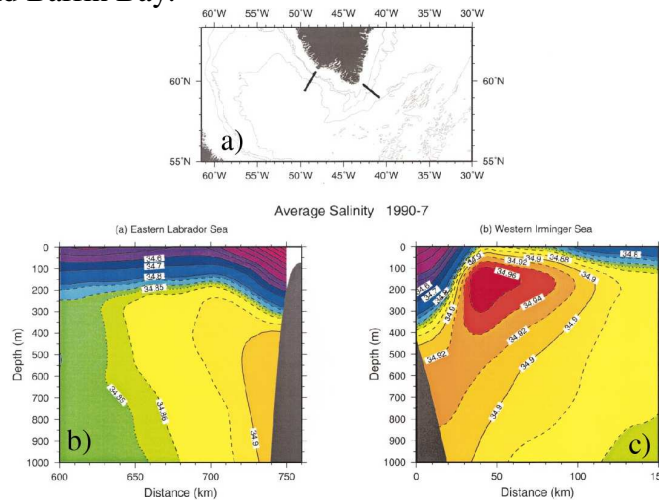

Figure 4. Mean upper-layer salinity sections for the period 1990–1997. a) Location of the two sections. Isobaths shown: 1000, 2000 and 3000 m. b) Eastern Labrador Basin. c) Western Irminger Basin. From Pickart et al. (2002).

On the fishing banks off West Greenland IW and PW dominates, as sketched in Figure 5. PW is continuously diluted by run-off from the numerous fjord systems. As the WGC reaches the latitude of Fylla Bank it branches. The main component turns westward and joins the Labrador Current on the Canadian side, while the other component continues north through Davis Strait.
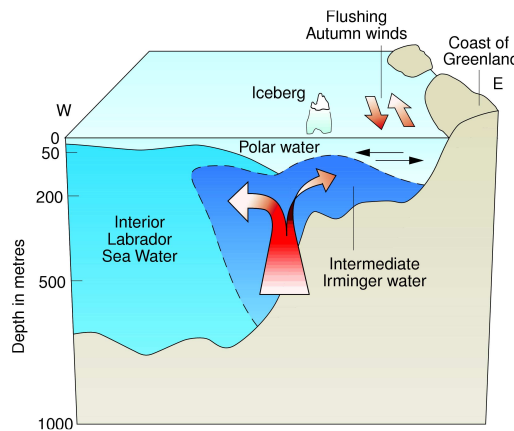

Figure 5. Sketch of the water masses off West Greenland in the Davis Strait region. From Valeur et al. (1997).

Off Southwest Greenland centred at about 61.5°N a source for of high eddy variability is found (Figure 6). These eddies are locally formed in the boundary current and propagates towards the interior of the Labrador Basin (Cuny et al., 2002; Lilly and Rhines, 2002; Prater, 2002; Pickart et al., 2002; Jakobsen et al., 2003). They mix water from the West Greenland shelf into the interior of the Labrador Basin. This has the effect, that the currents transporting IW and PW are extended much further offshore over deep water at West Greenland, contrary to the currents on the eastern side of Greenland, which are trapped to the shelfbreak (Figure 4; Pickart et al., 2002). The continental slope is particularly steep which is believed to be responsible to the high eddy kinetic energy in this specific place (Cuny et al., 2002; Buch, 2002). Baroclinic instabilities are formed at the front between the Irminger Water and the surrounding water masses and the intensity of the eddy activity is varying in time with the strength of the Irminger Current (Prater, 2002, Lilly and

Rhines, 2002).

There is no literature available that describe the importance of these eddies for the transport of fish larvae and nutrient loads off West Greenland. But it seems natural, that an offshore transport would have a negative influence on pelagic fish larvae. This remains to be investigated in detail, e.g. by a coupled oceanographic, biologic and chemical field study.
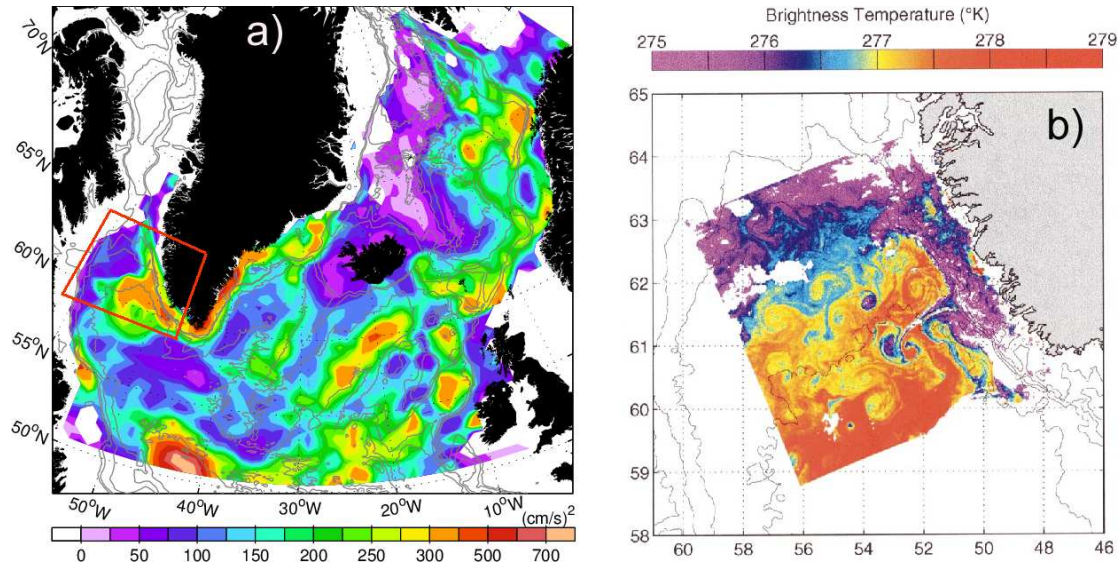
Figure 6. a) Distribution of eddy kinetic energy $0.5(<u'^2>+<v'^2>)$ calculated from high-pass filtered drifter data. Note the changing in scales at 300 cm²/s². Bottom topography lines at 500, 1000, 2000, 3000 and 4000 m is shown. Reproduced after Jakobsen et al. (2003). b) Sea surface brightness temperature of the northern Labrador Basin marked by red square on a). Bottom topography lines at 500, 1000, 2000 and 3000 m is shown. From Prater (2002).

Figure 7. (a) Bathymetry, (b) Modelled barotropic mean currents (April to November) at West Greenland in 2000 and (c) the sum of the barotropic and baroclinic currents all at 50 m depth. Overlayed on the panels are trajectories of 2 WOCE-SVP drifters drogued at 30 m. From Ribergaard et al. (2004).

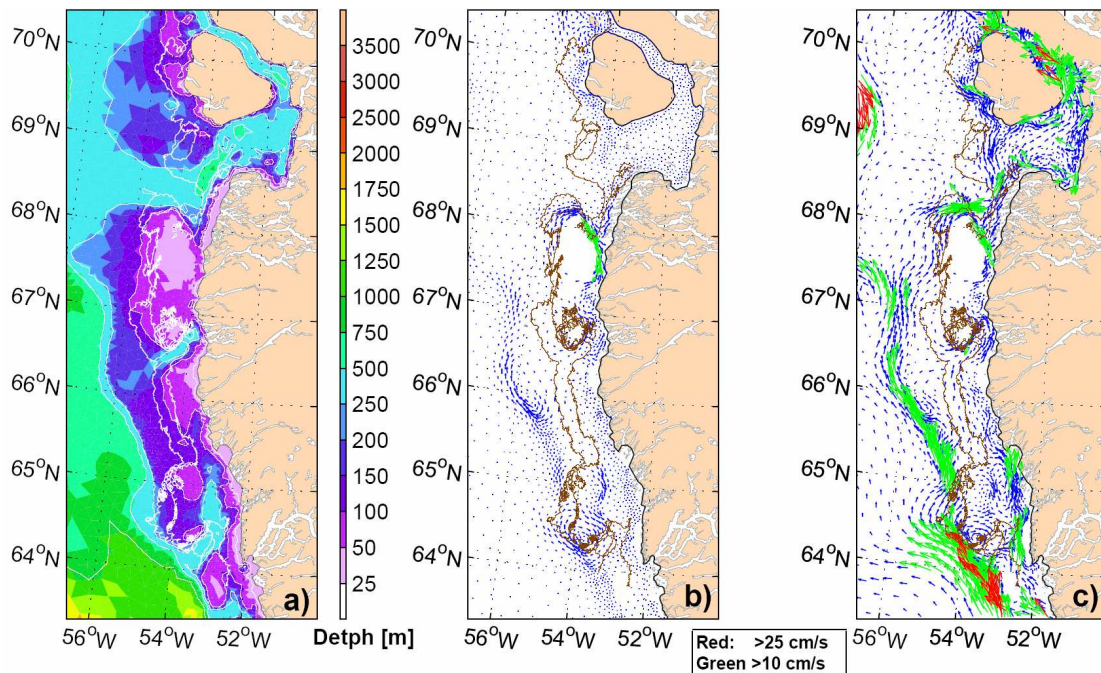Over the shelf off West Greenland a totally different form of eddies is found (Figure 7) as described by Ribergaard et al. (2004). Here the formation of the permanent eddies is a result of the interaction between the complicated topography and the strong tidal currents in the area giving rise to a residual current around the banks. This can be explained by the concept of topographic steered flow. As a consequence of conservation of potential vorticity, the flow tends to follow isobaths with shallower depths to the right. When the tidal flow is northward the current thus strengthen on the western side of a bank. Vice versa when the tide changes and flow is southward, the current strengthen on the east side of the same bank, and the mean flow is thus clockwise around the bank. The same argumentation gives counter-clockwise eddies around trenches. The most active area of permanent eddies is found between Fylla Bank (64°N) and Store Hellefisk Bank (68°N) where the tides are strongest.

At West Greenland the strongest tidal signal is located close to Nuuk at 64°N. The tides are primarily semidiurnal with large difference between neap and spring (1.5 m versus 4.6 m at Nuuk, Buch, 2002). Therefore the intensity of the anticlockwise circulation around the banks on the shelf will vary with a period of about fourteen days, as the strength of the barotropic tidal current and the tidal elevation is directly related.
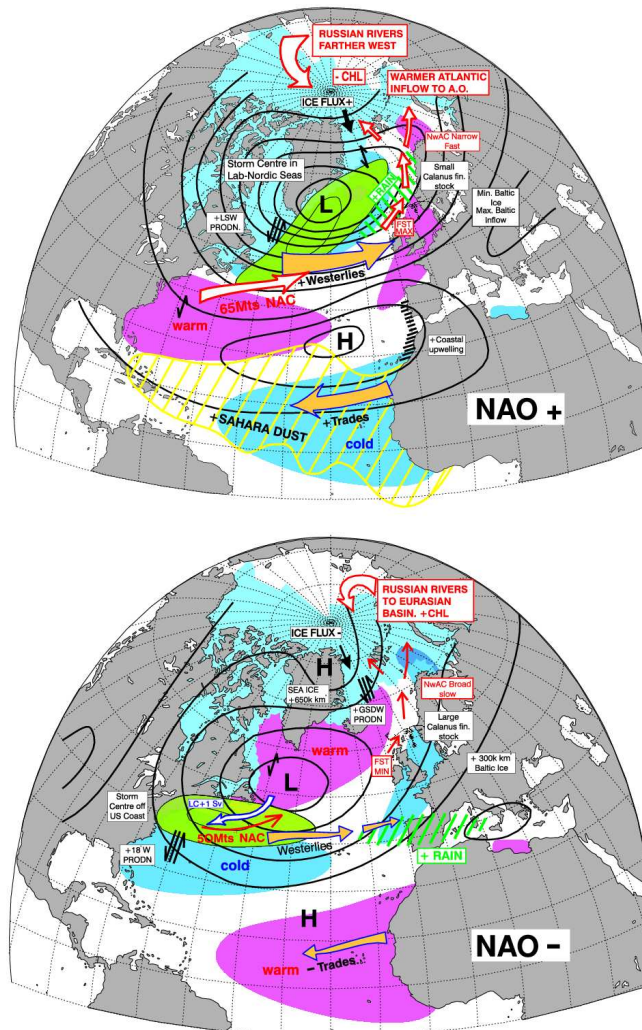

Figure 8. Schematic characteristic during high NAO index (upper) and low NAO index (lower). Modified from CLIVAR transparency D1 (courtesy of CEFAS, UK).
http://www.clivar.org/publications/other_pubs/clivar_transp/d1_transp.htm

Atmospheric variability in Southeast and West Greenland

The North Atlantic marine climate is largely controlled by the so-called North Atlantic Oscillation (NAO), which is driven by the pressure difference between the Azores High and the Iceland Low pressure cells (Figure 8). It is the most prominent mode of variability in the North Atlantic winter climate (Hurrell, 1995). Because the signature of the NAO is strongly regional, a simple index of NAO is commonly defined as the difference between the SLP anomalies at the Azores and Iceland (van Loon and Rogers, 1978 and references therein). Storm activity in the subpolar North Atlantic is strongly related to the NAO wintertime index (Hurrell, 1995). A positive index is associated with a more northeasterly storm track (Jones, 1990). We use wintertime (December–March)[1] sea level pressure (SLP) difference between Ponta Delgada, Azores, and Reykjavik, Iceland, and subtract the mean SLP difference for the period 1961–1990 to construct the NAO anomaly (Figure 9).
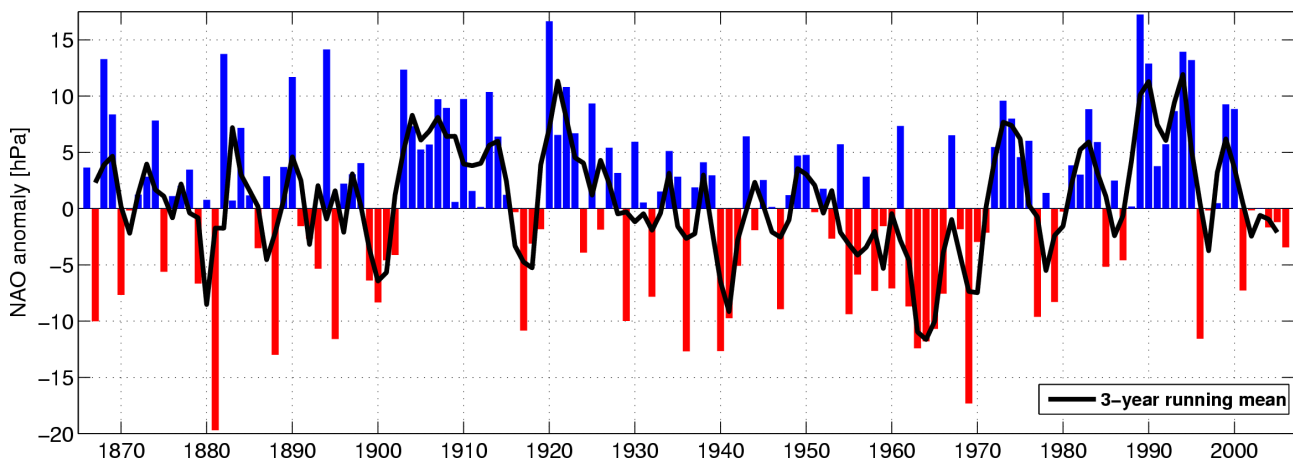

Figure 9. Time series of winter (December–March) index of the NAO from 1865–2006. The heavy solid line represents the meridional pressure gradient smoothed with a 3-year running mean filter to remove fluctuations with periods less than 3 years. (Data updated, as described in Buch et al., 2004, from http://www.cru.uea.ac.uk/cru/data/nao.htm.

The NAO is known to have a great impact on the ocean circulation and on the hydrographic conditions in the North Atlantic region including the Greenland Waters (e.g. Dickson et al., 1996; Dickson et al., 2000; Blindheim et al., 2000; Blindheim et al, 2001; Buch et al., 2004). Following Blindheim et al. (2000; 2001), the NAC is narrowed but strengthened during periods of high NAO. This is caused by the increased wind-stress as sketched on Figure 10a. Contrary, in periods of low NAO the NAC is widening and the branching is increased (Figure 10b). Noticeable is the increased Irminger Current. The relation, if any, between the NAO and the transport of the EGC is more uncertain.

The variability of the NAO index since 1865 is shown in Figure 9. Positive values of the index indicate stronger than average westerlies over the mid-latitudes associated with low-pressure anomalies over the region of the Icelandic Low and anomalous high pressures across the subtropical Atlantic.

During phases of high NAO index, the westerlies are amplified. Due to the maritime influence, the temperature over northern Europe becomes higher than normal. Similar, continental air masses from

---

[1] Others using December–February for constructing the NAO index.

northern Canada lower the mean temperatures over the Labrador Basin and at Southwest Greenland, as sketched in Figure 8a. Hurrell and van Loon (1997) showed that the temperature anomalies for the North Atlantic and surrounding land masses for the 1980–1994 period was strongly related to the persistent and exceptionally strong positive phase of the NAO. Similar, Hanna and Cappelen (2003) showed, that the cooling in the coastal southern Greenland region from about 1970 was significantly inversely related to an increased positive phase of NAO. Box (2002) even found the NAO to be highly significant related to the temperatures on the coast at western and southern Greenland for the period 1873–2001. This clearly demonstrates a strong correlation between the strength of the westerlies across the North Atlantic (the NAO index) and the air temperatures in Greenland and Europe. Further it shows that the air temperatures in Greenland and Europe are negatively correlated, a phenomenon referred to as a seesaw effect (e.g. van Loon and Rogers, 1978).
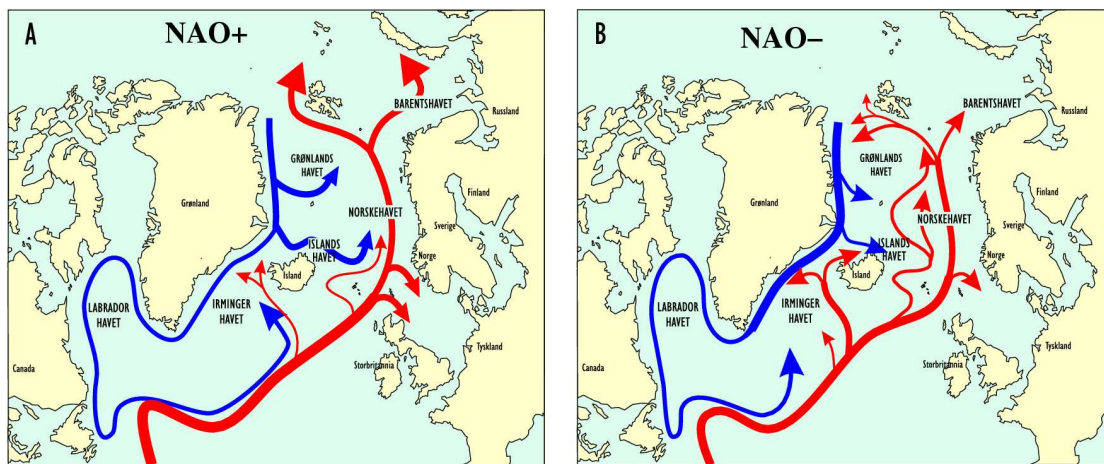
Figure 10. Schematic surface circulation during a) high NAO index, and b) low NAO index. From Blindheim et al. (2001).

This is further illustrated in Figure 11 which shows a comparison of the air temperatures over Greenland from a low NAO period (1960–1969) to a high NAO period (1990–1999). Note that especially offshore of West Greenland, but also over the Irminger Basin, it was significantly warmer in the 1960s than in the 1990s. Contrary, northern Europe but also the Greenland Basin offshore northeast Greenland was significant cooler in the 1960s than the 1990s.

Figure 11. Difference in air temperatures at the 1000 hPa level between 1960–1969 and 1990–1999 calculated using NCEP/NCAR reanalysis data (www.cdc.noaa.gov).

West and Southeast Greenland lies within the area which normally experiences warm conditions

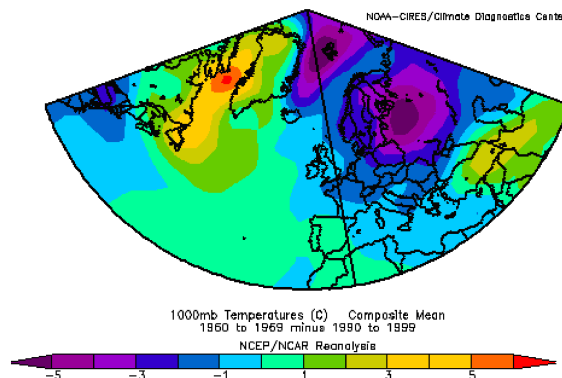when the NAO index is negative. As can be seen from Figure 12 the annual mean air temperature in Nuuk shows large interannual variations of 1–2°C but sometimes nearly 5°C. The temperature was generally very low from the start of the time series in 1873 to the early 1920s. In the mid-1920s the mean annual temperatures suddenly increased by about 1°C at stay high at this level until the late 1960s. Then the temperature became slightly lower, but interrupted by three cold periods centered about 1970, 1982–1984 and 1989–1994. From the mid-1990s the temperature has remained fairly stable with slightly lower temperatures than during the warm period.

On the southeast coast of Greenland, the temperature at Tasiilaq showed a similar history (Figure 12). However, the interannual variations are in general much lower around 0.5°C. The regime shifts in temperature are much more evident in this time series. The cold period at the start of the time series came to an end between 1925 and 1926 whereas the warm period was interrupted by a decrease in temperature between 1964 and 1966. The following cold period was more evident at Tasiilaq than at Nuuk. A return to warmer climate conditions is seen from 1996. After 2000 the temperatures reached similar high values as in the previous warm period.

These temperature variations are closely linked to the NAO index. At about 1925 the NAO index shifted from a generally positive phase to generally negative phases, which culminated in the mid-1950s and the 1960s. In the same period both Nuuk and Tasiilaq experienced warm conditions. High NAO values in the early 1970s, the early 1980s and the early 1990s are clearly reflected in temperature drops. However, after the mid-1990s the temperatures were fairly high despite of high NAO values. This was due to a displacement of the Icelandic low-pressure cell towards the northeast (ICES, 2000, 2001, 2002). In 2003 the low-pressure cell was displaced towards southwest and the high pressure-cell towards northeast resulting in a northwestward wind anomaly over the Iceland and Irminger Basins (Ribergaard and Buch, 2004). Therefore it should be stressed, that using NAO as an indicator for the climate at West Greenland should be done with caution, as the positions of the high-pressure and especially of the low-pressure cell varies over time.
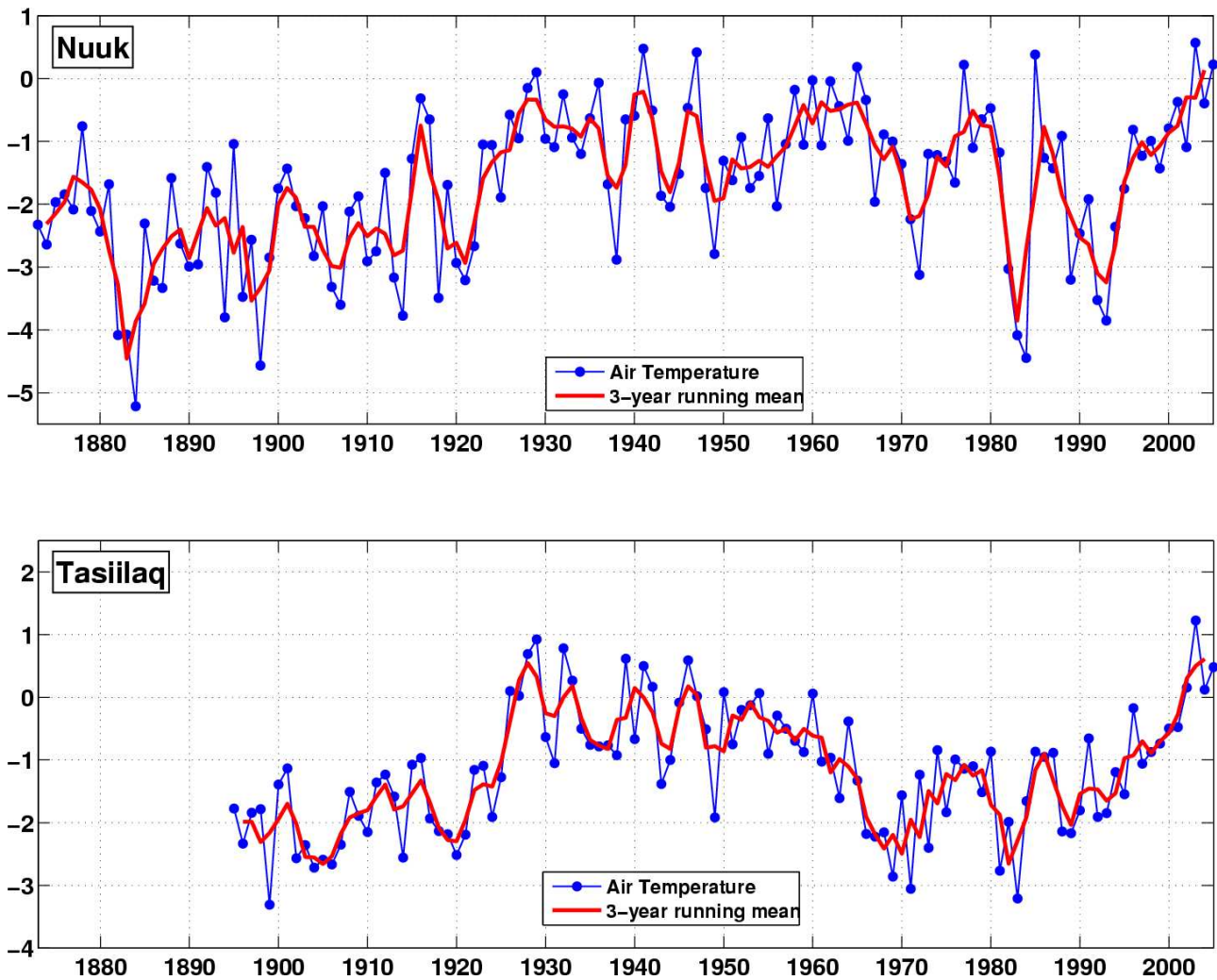
Figure 12. Annual mean air temperature southwest (Nuuk) and southeast (Tasiilaq) of Greenland for the period 1873–2005 See Figure 1 for location. From Ribergaard (2006).

Hydrographic variability off Southwest Greenland

Changes in the ocean climate off West Greenland generally follow those of the air temperatures. Exceptions are years with great salinity anomalies i.e. years with extraordinary inflow of Polar Water (Dickson et al., 1988, Belkin et al., 1998; Belkin, 2004).

The mid-June mean surface (0–40 m) temperature and salinity on top of Fylla Bank st. 2 is shown in Figure 13. They show large interannual variations, sometimes by more than 1°C in temperature and 0.5 in salinity. The 3-year running mean better reflects the large scale climate variations, because it smoothes out the high-frequently variations. Warm conditions were observed in the period 1950–1968. Around 1970 the temperature drops to the coldest period experienced due to an anomalous high inflow of Polar Water, which was closely linked to the "Great Salinity Anomaly" (Dickson et al., 1988, Belkin et al., 1998) and is clearly reflected in the salinity. At the same time, a shift to cold atmospheric conditions was observed reflecting the shift from negative to positive NAO values. In the early 1980s and early 1990s additional two cold periods were observed both in the atmosphere and the ocean reflecting the local cooling due to high NAO conditions. During the late 1990s higher ocean temperatures are observed despite of high NAO values, which were caused by a northeastward displacement in the low pressure cell. In 2003 a displacement of the low-pressure cell towards southwest and the high-pressure cell towards northeast resulted in anomaly

southwesterlies winds over the Iceland and Irminger Basins causing the East Greenland Current through Denmark Strait to weaken and the Irminger Current to strengthen (Ribergaard and Buch, 2004). In 1997 low ocean temperature was observed despite quite warm atmospheric conditions. Low salinities suggest that this was due to a high inflow of Polar Water.
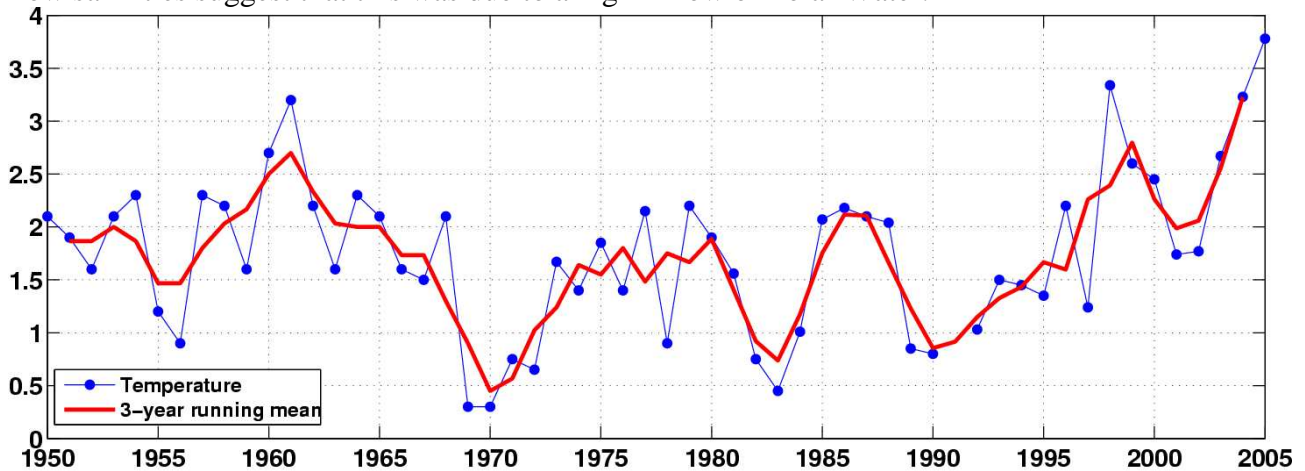

Figure 13. Mid-June mean surface (0–40 m) temperature (top) and salinity (bottom) on top of Fylla Bank st. 2. for the period 1950–2005. From Ribergaard (2006).

Similar ocean temperature history is seen at the continental slope west of Fylla Bank in the upper 400 m (Fylla Bank st. 4, Figure 14). The core of the IW is found in the depth interval from 400–600 m. A clear decrease in the salinity and temperature in the end of the 1960s indicate a reduction of the inflow of IW to the area as expected for a change from negative to positive NAO values (see Figure 9). Increasing temperatures are measured from the second half of the 1990s, but the salinities did not increase until the end of the 1990s. The same trend is also seen at a section off Cape Farewell (Buch et al., 2004), but here the salinity did increase form the mid-1990s. Similar variations were reported by Mortensen and Valdimarsson (1999) south of Iceland indicating increased strength of the Irminger Current since the mid-1990s. This relative long period of stable warm conditions may be beneficial for species like the Atlantic cod though the temperatures are slightly lower than in the warm 1960s.
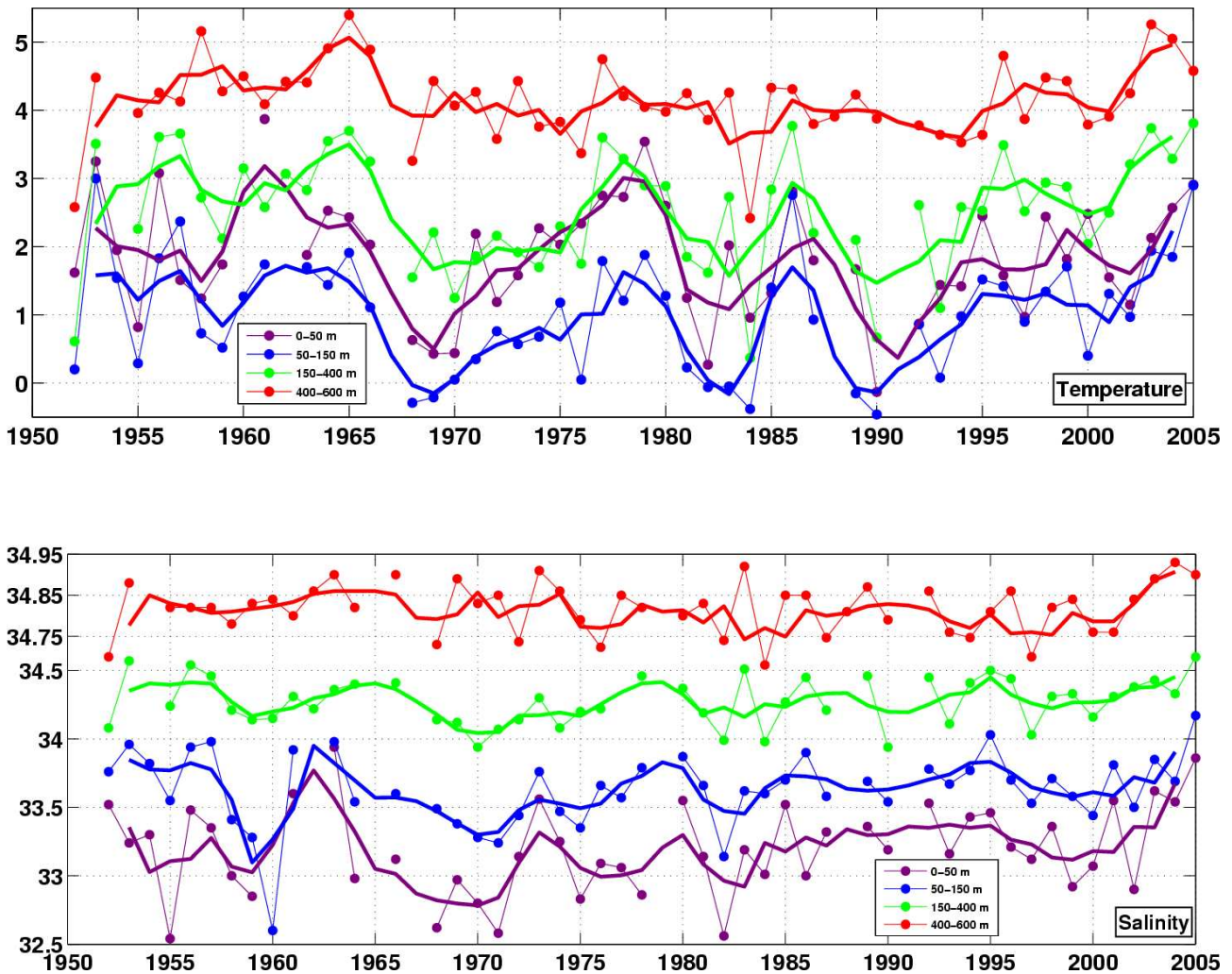
Figure 14. Mean temperature (top) and salinity (bottom) for the period 1950–2005 n four different depth intervals west of Fylla Bank (st. 4) over the continental slope. Note the change in scales at 34.75 for salinity. From Ribergaard (2006).

Sea ice and its variability

Sea ice is important in Greenland waters. At West Greenland two different types of sea ice dominate.

West-ice is first-year ice formed in Baffin Bay and Davis Strait. It normally does not affect the Southwest Greenland waters, because the inflow of warm IW within the West Greenland Current peaks in late autumn and early winter and limits its extent to the northern Hellefisk Bank (Buch, 1990; see Figure 1 for location). However, during cold periods its distribution is extended further south. The low temperatures in the around 1970, the early 1980s and the early 1990s are clearly reflected in the west-ice coverage (Figure 15).
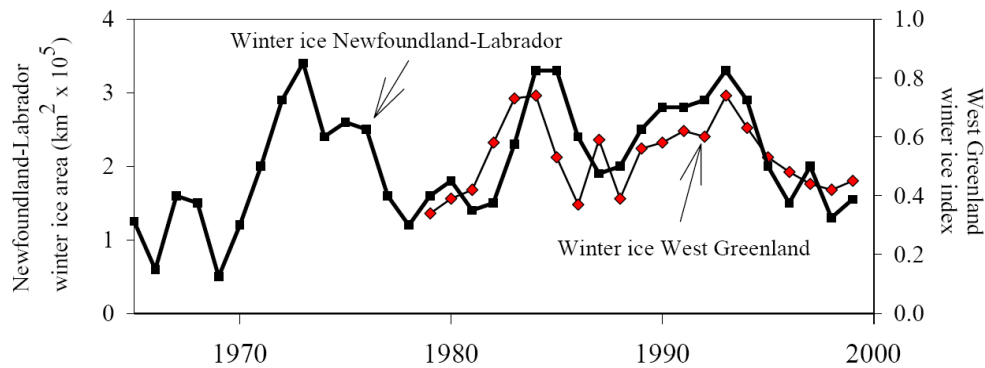
Figure 15. Area of winter (January–March) ice cover (km²) off Newfoundland-Labrador, 1963–1999 from Drinkwater *et al.* (2000) and area index of winter (January–February) ice cover "West-ice" off West Greenland (62°N–70°N) from Leif Toudal Pedersen, Danish Technical University. From Buch et al. (2004).

Multi-year ice ("storis") dominates in the southern part of West Greenland and is present 8–9 month a year in the Julianehaab Bight from Cape Farewell to about 61°N. It is originating from the Arctic Ocean and is carried to Southwest Greenland by the East Greenland Current. The amount of multi-year ice entering West Greenland waters shows great interannual variability as well as variations on multi-decadal timescales (Schmidt and Hansen, 2003). The mechanism behind the multidecadal variations is poorly understood, but may be linked to the circulation within the Arctic Ocean. The interannual variability is controlled by several factors such as outflow of sea ice from the Arctic Ocean, formation of sea ice along the northeastern coast of Greenland and in the Greenland Sea, and wind conditions over the Greenland and Irminger Basins and over the Iceland Plateau. Extreme amount of multi-year ice entered West Greenland waters in 1968–1970, 1982, 1984, 1989, 1990 and 1993 (Keld Q. Hansen, Danish Meteorological Institute, Center for Ocean and Ice, personal communication).

3. Numerical model

Simulations

Hydrodynamic simulations are performed for the West Greenland shelf with a special focus on the shelf region off Disko Island and Disko Bay. The aim is to simulate the ocean state, i.e. ocean currents, temperature, salinity, ice cover, etc. in a one year period in order to investigate the typical conditions and extreme event at different seasons. Further, the simulations provides the forcing fields for oil spill simulations described in Nielsen et al. (2006). The simulation period is from July 1, 2004 to July 1, 2005.

Model description

The simulations are performed with the Hybrid Coordinate Ocean Model (HYCOM). The model is described in detail by Bleck (2002), and online information is found at http://hycom.rsmas.miami.edu. It is a primitive equation ocean general circulation model which solves the three-dimensional prognostic equations for horizontal velocity, continuity (giving elevation and layer thickness), salt and temperature.

The vertical coordinate is generalized. In the hybrid configuration the vertical coordinate is isopycnal in the open, stratified ocean, but smoothly reverts to a terrain-following coordinate in shallow coastal regions, and to z-level coordinates in the mixed layer and/or unstratified seas. This makes the model suitable for simulations of the open ocean as well as shallow coastal seas and unstratified parts of the world ocean.

Tidal forcing is included as a body tidal potential. This means that the tidal wave is generated within the model domain. The routines for tide generation has been developed at NCEP/NOAA.

The model includes a thermodynamic representation of sea ice, but sea ice dynamics (ice drift) is lacking. This is a reasonable approach for the Baffin Bay and Labrador Sea, i.e. for the Mid- and North West Greenland coast.

Model setup

The model setup is (always) a compromise between the available computer resources and number of grid point necessary to provide sufficiently high resolution for the area of interest. In this study we are interested in the ocean conditions off West Greenland. As described in Chapter 2, the large scale current system in the North Atlantic strongly influence the study area. Therefore, the demands for the model setup are a high resolution on the West Greenland shelf and a good description of the North Atlantic current system. The model is thus set up in a series of three one-way nested domains with increasing resolution. The boundaries of the domains are shown with red lines in Figure 16. The largest domain (in the following called the NAT-domain) covers the entire Arctic Ocean and North Atlantic north of approx. 20°S. It has 206×116 grid points and a resolution of approximately 50 km and serves to provide boundary conditions for the region of interest. The horizontal grid used is a rotated Mercator projection with the rotated equator along 30W longitude.

The waters around Greenland are covered in the second nesting domain (called the GRL-domain) with 311×241 grid points and a resolution of approximately 10 km. This domain provides the ocean forcing fields for the oil spill simulations described by Nielsen et al. (2006), and it is the primary domain in this study. The domain includes the entire shelf around Greenland, most of the Canadian Archipelago, the Baffin Bay, the Labrador Sea, the Irminger Basin, Denmark Strait, and half of the Iceland and Greenland Sea including the Fram Strait. The rationale for applying the high resolution also east of Greenland, even though we in this study are interested in the shelf off the west coast only, is that the East Greenland Current and the Irminger Current feed into the West Greenland Current and thus control the hydrographic conditions off West Greenland.

Finally, a third nesting domain (called the DIS-domain) has 161×141 grid points and a resolution of approximately 2 km and cover the entire Disko Bay area. It is used to provide a better description of upwelling areas where nutrients are being brought to the surface layer from greater depths, which is of great importance for biological activity. Upwelling usually takes place on small horizontal length scales constrained to the bathymetry, or in case of wind driven upwelling along the coast or the ice-edge. In order to simulate these processes correctly a very high resolution is necessary.

The nesting procedure is one-way. This means that the simulations are performed sequential and that output from the larger domain is used as boundary condition for the smaller domain, but there is no feedback of information from the smaller domain to the larger.
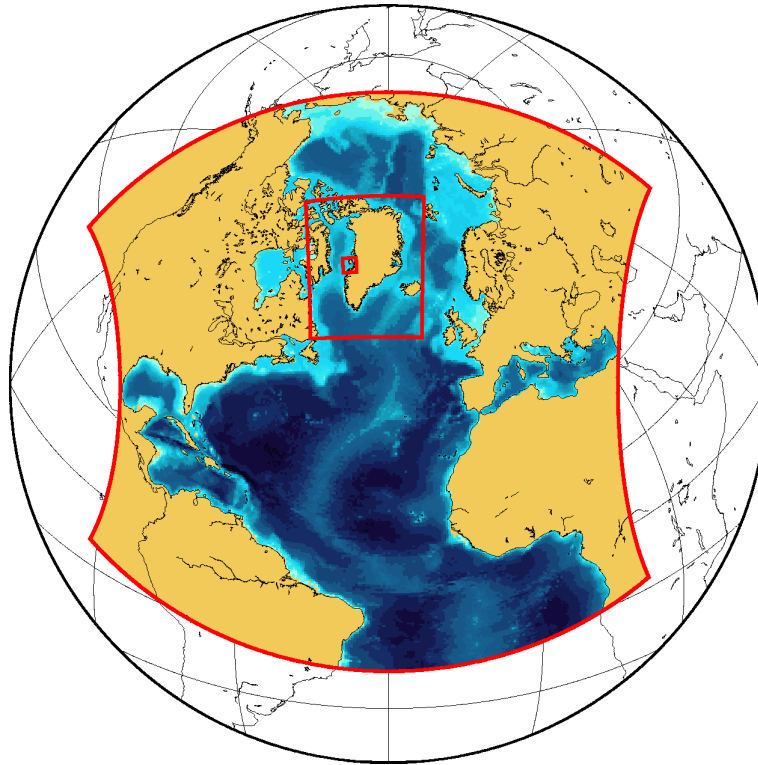
Figure 16. Model domains. The large domain (NAT) covers the North Atlantic and Arctic Ocean, the second nesting domain (GRL) covers the waters around Greenland, while the third and smallest domain (DIS) covers the Disko Bay.

The GRL-domain is configured with 26 layers, with potential density (σ_θ) values of 20.00, 21.50, 23.00, 24.00, 24.70, 25.28, 25.77, 26.18, 26.52, 26.80, 27.03, 27.22, 27.38, 27.52, 27.63, 27.71, 27.77, 27.82, 27.86, 27.90, 27.94, 27.98, 28.01, 28.04, 28.07, and 28.10. For the NAT domain, 3 additional layers, 28.40, 28.70, 29.00, has been included in order to represent deep Mediterranean Water. Only the 18 lightest layers for the GRL domain is used for the DIS-domain, since the heavier densities represent water masses which are not found within the DIS domain. Since the upper ocean is our primary interest in this study, we use potential density (σ_θ) with respect to surface reference pressure.

Input data

The model is initialized with high resolution (1/4°) climatological temperature and salinity fields[2] by Boyer et al. (2005). These fields are also used for the relaxation procedure of the surface temperature and salinity described below.

Atmospheric forcing fields consists of surface wind stress, 10m wind speed, surface air temperature, precipitation, water vapor mixing ratio, and short- and long-wave radiation heat fluxes. The fields are taken from the DMI numerical weather prediction model DMI-HIRLAM-T (Yang et al., 2005) covering a large part of the northern hemisphere with a 0.15 degree resolution (see Figure 17). The fields are given with a 1 hourly interval. For the southern part of the North Atlantic, which is not covered by HIRLAM, fields from the global weather prediction model at ECMWF[3] are used. Forcing fields from the two atmospheric models merge well, since DMI-HIRLAM-T uses fields from ECMWF as boundary conditions.

---

[2] Data and information online at www.nodc.noaa.gov/OC5/WOA01/qd_ts01.html
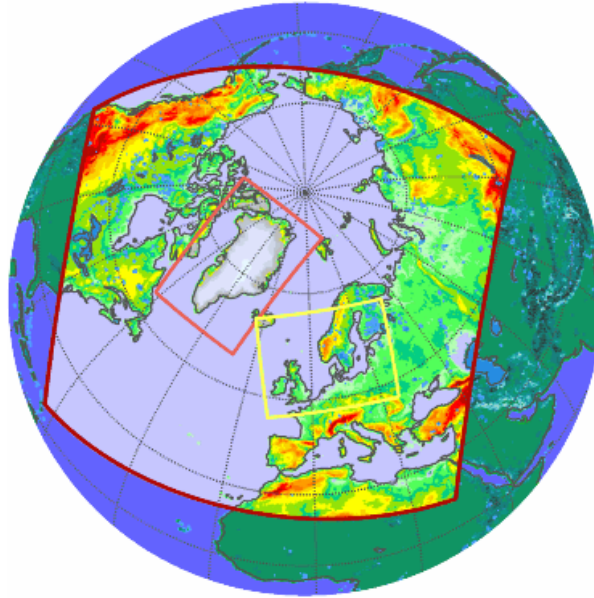[3] European Centre for Medium-Range Weather Forecasts (www.ecmwf.int)

Figure 17. DMI-HIRLAM domains.

Some of the atmospheric forcing fields are diagnosed from the HIRLAM and ECMWF model output. Surface wind stress is calculated as

$$\tau = \rho_a C_d |\mathbf{v}| \mathbf{v}$$

where ρ_a is the air density, $\mathbf{v}$ is the velocity vector, and C_d is the drag coefficient, depending of the wind speed as

$$C_d = \min(2.7 \cdot 10^{-3}, 10^{-3} + 0.85 \cdot 10^{-4} \cdot |\mathbf{v}|)$$

Radiation heat fluxes are parameterized as described by Cheng (2002). The short-wave radiation flux Q_s is following Shine (1984) and Bennet (1982)

$$Q_s = (1 - 0.52C) \frac{S \cos^2 Z}{(\cos Z + 1.0) \cdot e \cdot 10^{-3} + 1.2 \cos Z + 0.0455}$$

where C is cloud cover, S is the solar constant, Z is the local solar zenith angle and e is the vapour pressure. The downward long-wave radiation is following Prata (1996) and Jacobs (1978)

$$Q_d = (1.0 + 0.26C)\left(1.0 - (1.0 + \eta) \cdot \exp(-\sqrt{1.2 + 3.0 \cdot \eta})\right)\sigma T_a^4$$

where σ is the Stefan-Boltzmann constant, T_a is the air surface temperature, and $\eta = 46.5 \cdot e / T_a$.

River runoff data is applied in the NAT-domain as monthly climatological discharges from the 115 largest river discharge stations of the Global Runoff Data Centre (GRDC)[4] and scaled as in Dai and Trenberth (2002). One single freshwater discharge is added in the southern Kattegat, Denmark, representing the Baltic Sea replacing the GRDC rivers supplying the Baltic Sea.

---

[4] http://grdc.bafg.de

No freshwater discharge climatology exists for the large Greenlandic fjords, but the discharge from the Greenland ice cap has been parameterized. Since no data was available this is done in a simple manner, by having five freshwater sources along the Greenland coast, each having a seasonal variation with a maximum release of 414 m^3/s in July and August and zero during wintertime. The sources are located at (51.5W;69.2N), (51.9W;63.8N), (46.3W;60.5N), (26.9W;71.5N), (52.7W;71.7N). The values are somehow adapted from Box et al. (2004), but since this work only model annual fresh water runoff within large squares, we have converted the data into pseudo monthly discharges.

Spin-up

The simulation is spun up from an ocean at rest with initial temperature and salinity given by Boyer et al. (2005). The spin up period is one year (July 1, 2003 to July 1, 2004). The spin-up is performed on the NAT-domain solely, and interpolated to the GRL- and DIS-domain.

4. Results

Model results are saved in an extensive archive, with a one hour interval. Both two-dimensional barotropic fields such as elevation, barotropic velocities and sea-ice fraction, and three-dimensional baroclinic fields such as current, temperature and salinity are stored. In this chapter a few examples of model results are presented.

GRL-domain

While the large NAT-domain is too coarse to really resolve the Greenland shelf, the GRL-domain with a 10 km resolution is able to capture important topographic features such as the banks on the West Greenland shelf. Also the East- and West Greenland Current are resolved relatively well by the model. Figure 18 show salinity at 20m depth. The fields are snapshots of the model results taken the 16th in each month. The seasonal variation of the East Greenland Current is clearly seen, as is the seasonal variation in the Baffin Bay. Also, eddy activity along the East and West Greenland Current is seen.

The seasonal variation is even more pronounced in profiles. Figure 19 show profiles for temperature, salinity, and density at the position 53.0W, 69.2N in the entrance to the Disko Bay. The thin surface layer is formed in the late spring as a consequence of warming of the thin surface layer formed by melting of sea-ice and especially freshwater run-off. In the profiles it shows as a freshening and a warming of the surface layer starting in June. In August and September the surface layer is deepened, and during late fall a cooling takes place at the surface and the freshwater discharge from land disappears, and the surface layer is degenerated. During wintertime the surface layer is well mixed down to about 100m depth and the layer is cooled.

DIS-domain

One of the main reasons to perform the simulation on the DIS-domain, with the high resolution for the Disko Bay area, is to simulate the upwelling. In additional to wind driven upwelling, it takes place in confined areas constrained to the bathymetry. High fluctuation of up- and downwelling results in vertical mixing of the watermasses[5] and thereby nutrient can be added to the surface

---

[5] Can be seen in both temperature and salinity (not shown).

layers from below stimulation the biological activity. Figure 20 shows a map of standard variation of the vertical velocity at 20m depth for April-May 2005, indicating where up- and down-welling takes place. There is a large area on the northern and eastern side of Store Hellefisk Bank, which is also easily recognized in the GRL-domain (not shown), and which was first reported by Pedersen et al. (2005). Smaller up/down-welling areas are seen in a line across the Disko Bay. These are connected to the island groups of Hunde Ejland and Kronprinsens Ejland at the sill in the mouth of the Disko Bay. The islands are known to be surrounded by nutrient rich waters which attract both sea birds and whales. Also, some small areas along the coast of Disko Island is seen, as well as a larger area in the northern Vaigat. Parts of the open boundary also show large up- and downwelling activity, however this is most likely caused by the boundary conditions and therefore not physically real.
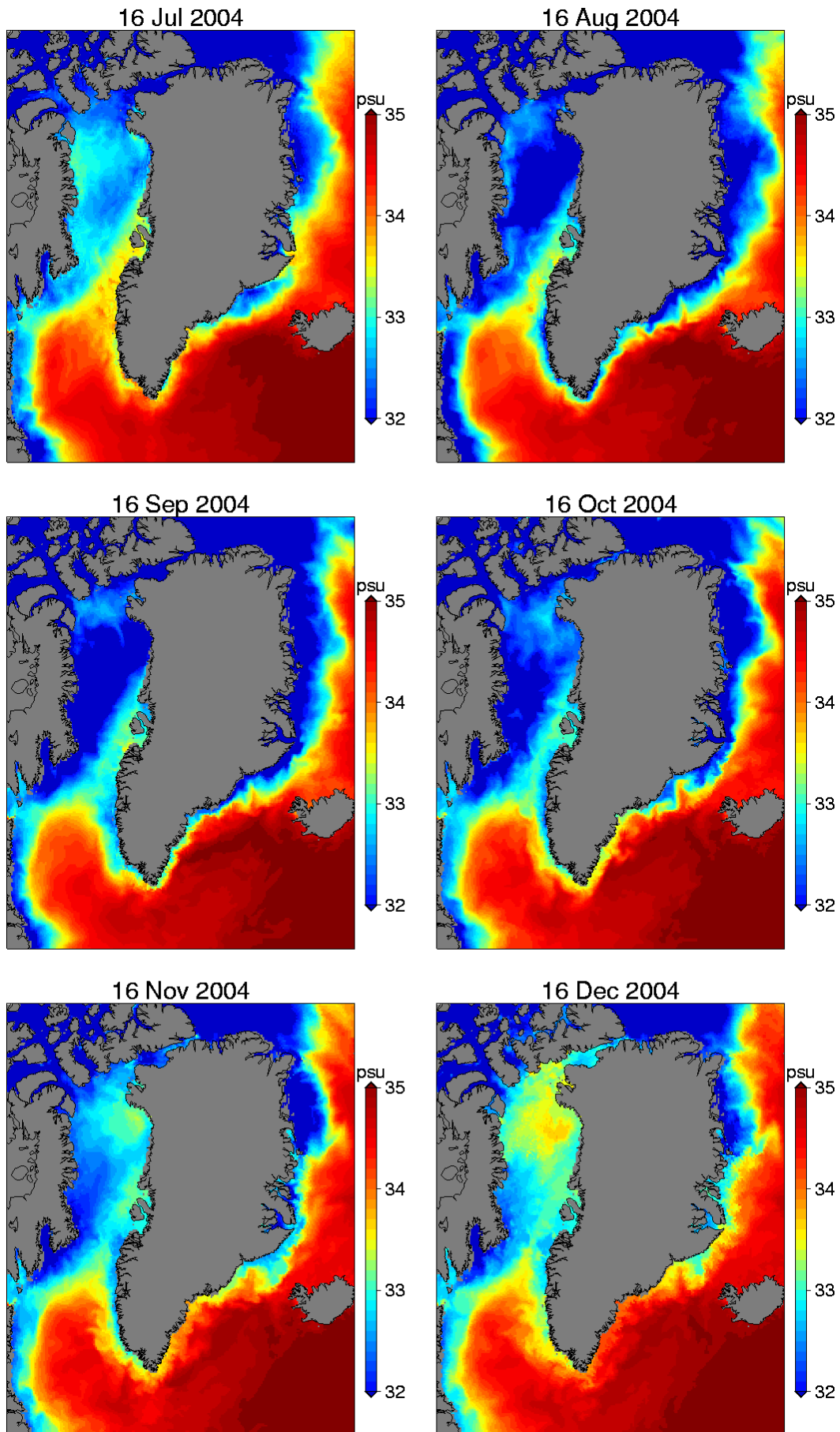
16 Jul 2004

16 Aug 2004

16 Sep 2004

16 Oct 2004

16 Nov 2004

16 Dec 2004

Figure 18. Salinity at 20m depth for the GRL domain.

16 Jan 2005

16 Feb 2005

16 Mar 2005

16 Apr 2005

16 May 2005

16 Jun 2005

Figure 18. Continued.

16 Jul 2004

16 Aug 2004

16 Sep 2004

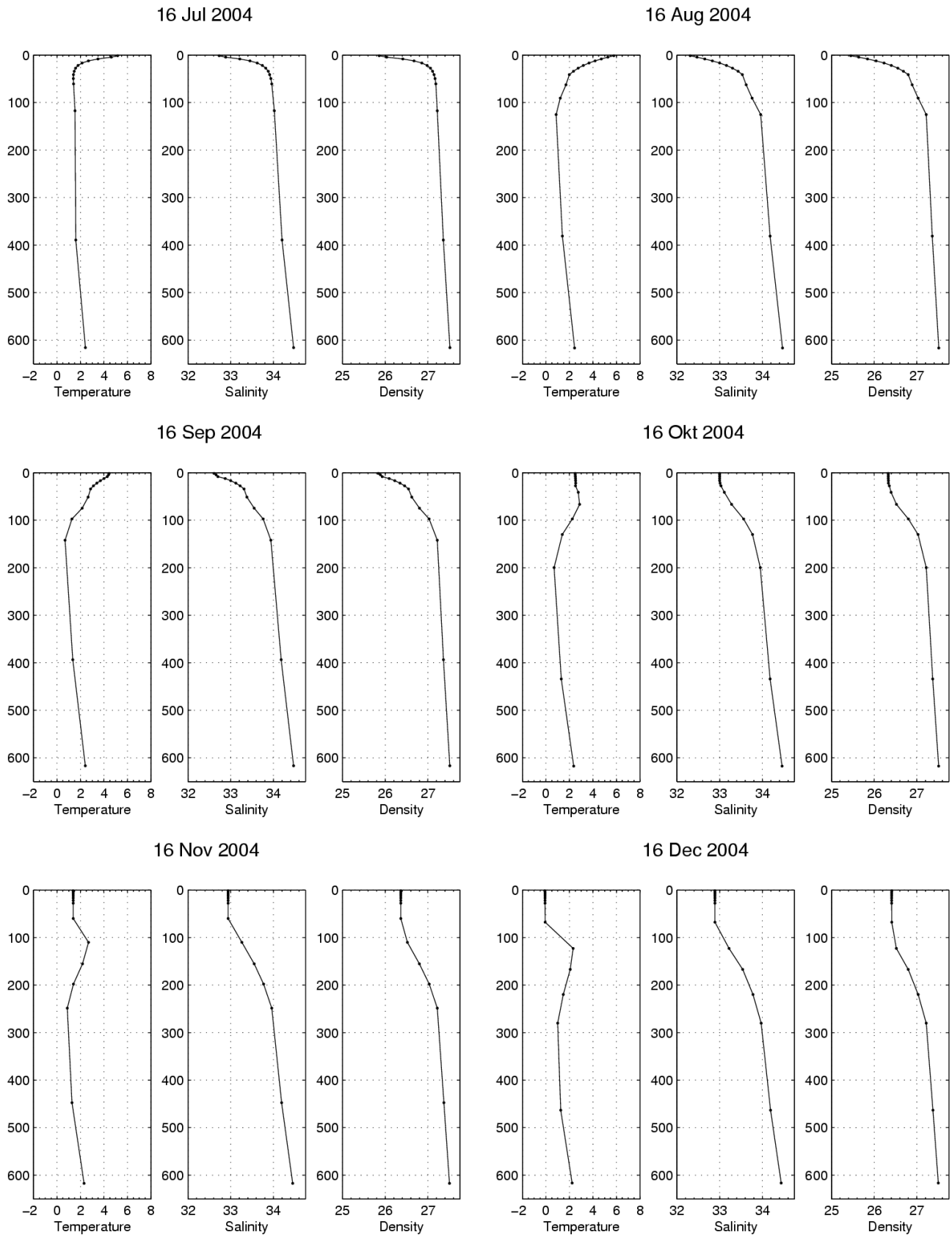16 Okt 2004
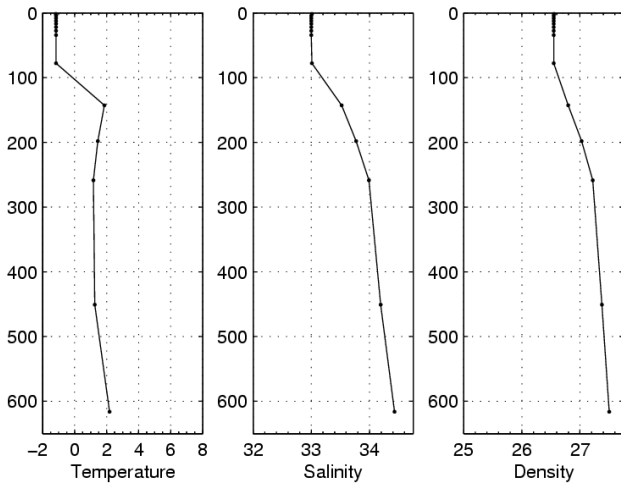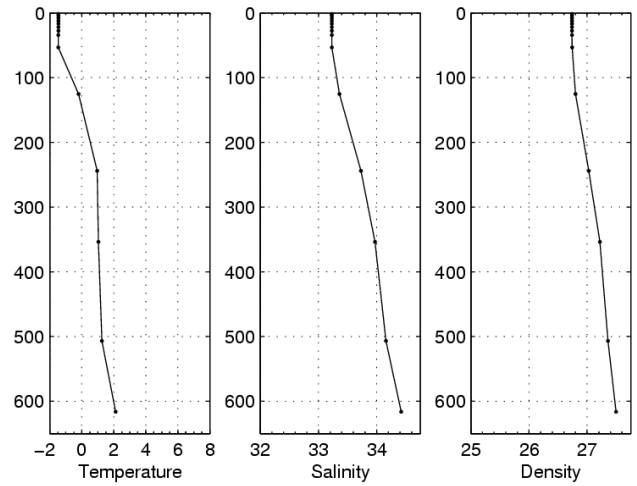
16 Nov 2004

16 Dec 2004
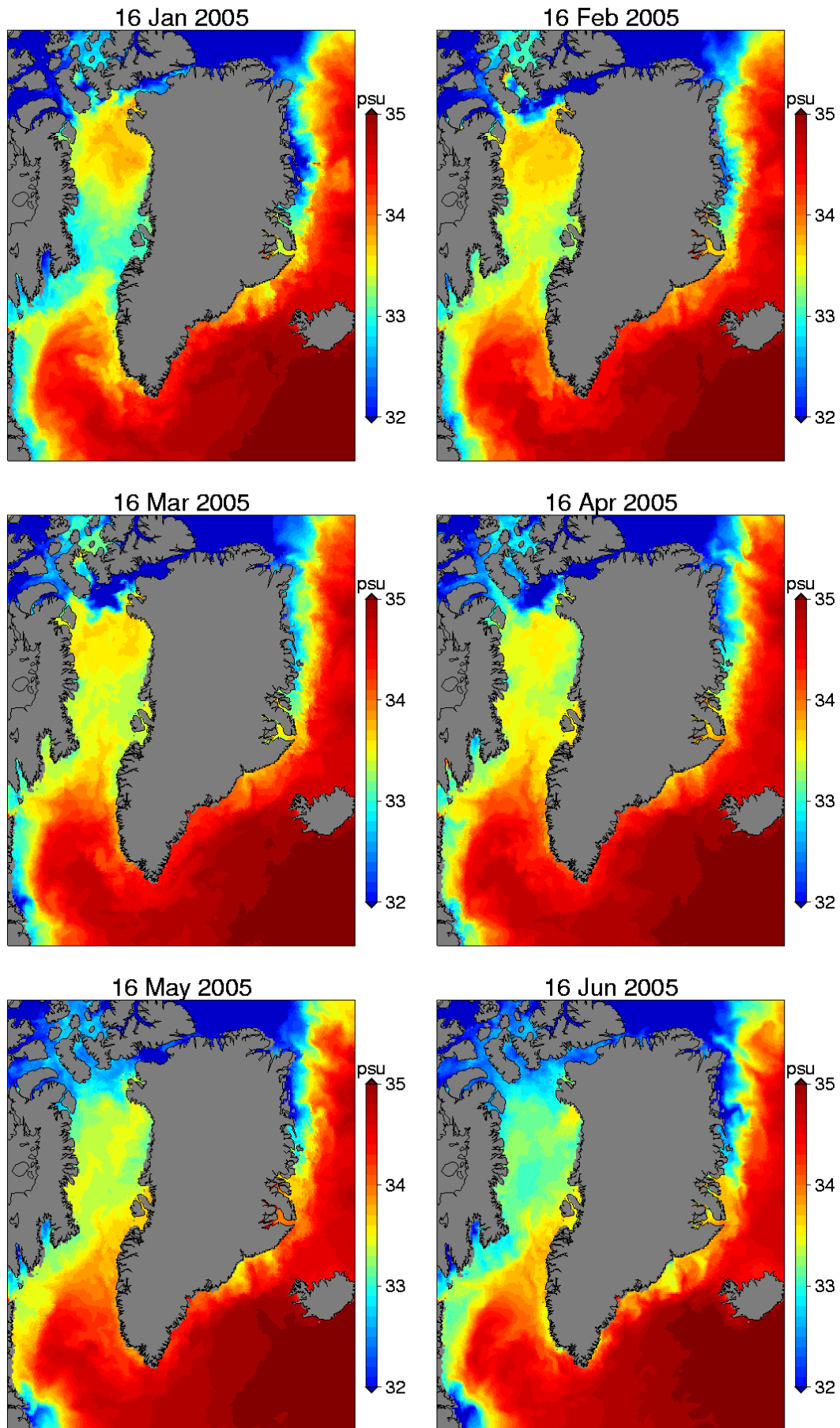
Figure 19. Potential temperature, salinity, and density profiles at 53.0W, 69.2N. The dots on the profiles is in the center of the each vertical model layer. Note it changes during time due to the stratification.
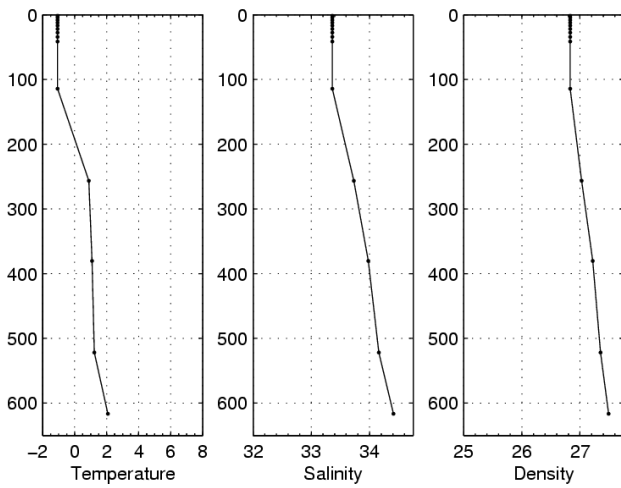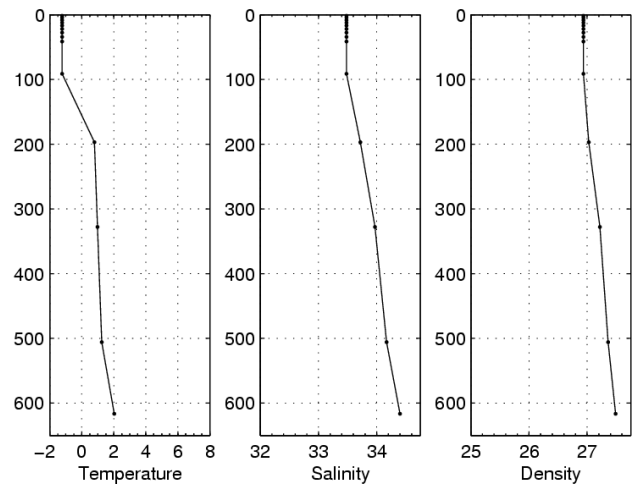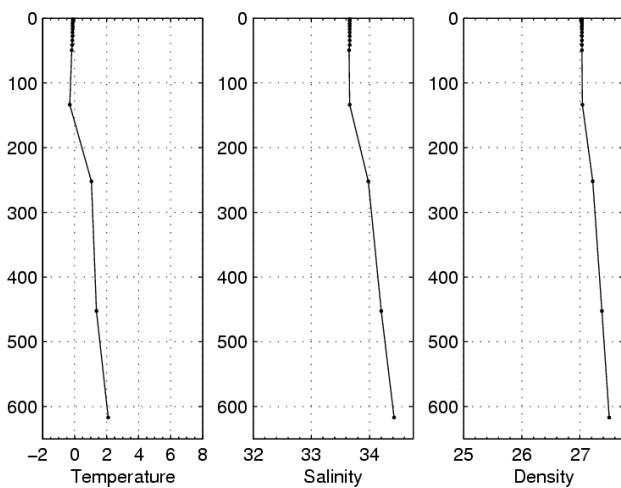
16 Jan 2005

16 Feb 2005
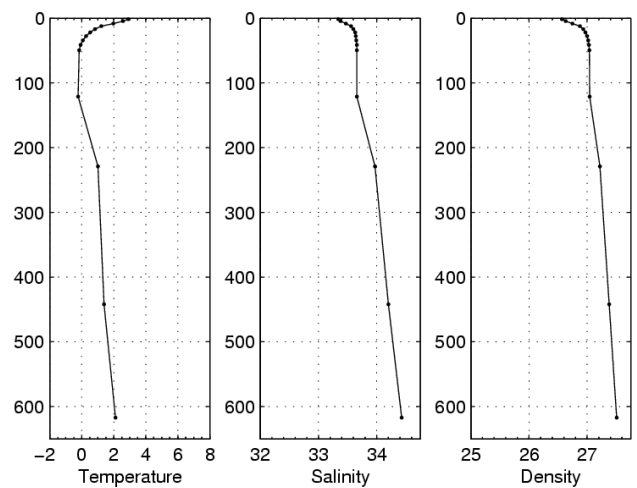
16 Mar 2005

16 Apr 2005

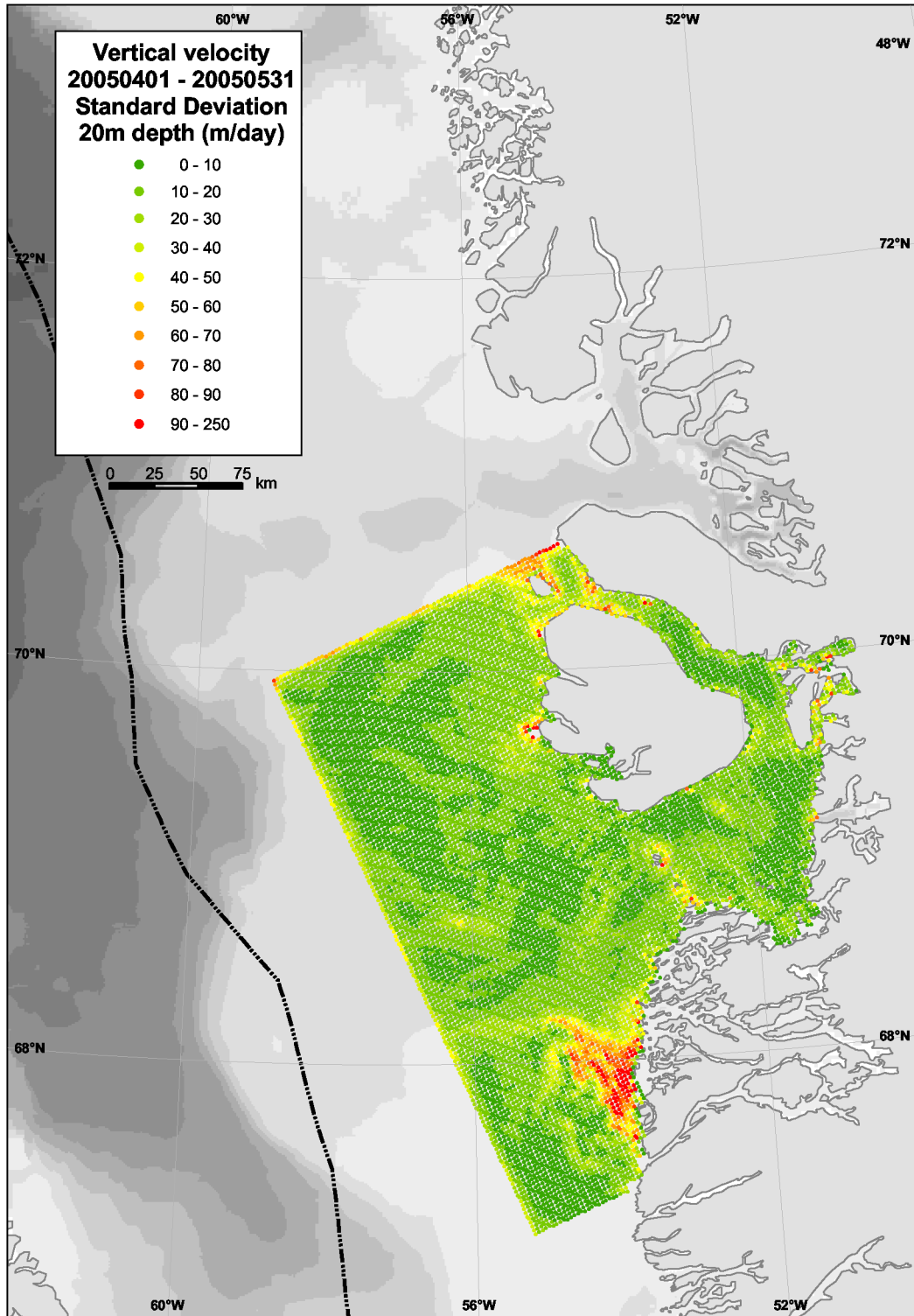16 May 2005

16 Jun 2005

Figure 19. Continued.

Figure 20. Standard variation of vertical velocity at 20m depth for April and May 2005 for the DIS-domain.

References

Belkin, I.M., 2004. Propagation of the "Great Salinity Anomaly" of the 1990s around the northern Atlantic. *Geophysical Research Letters* **31**, L08306, doi:10.1029/2003GL019334.

Belkin, I.M., Levitus, S., Antonov, J., and Malmberg, S.-Aa., 1998. "Great Salinity Anomalies" in the North Atlantic. *Progress in Oceanography* **41**, 1–68.

Bennet, T. J., 1982. A coupled atmospheric-sea ice model study of the role of sea ice in climatic predictability. *J. Atmos. Sci.* **39**, 1456–1465.

Bleck, R., 2002. An oceanic general circulation model framed in hybrid isopycnal-Cartesian coordinates. *Ocean Model*. **4**, 55–88.

Blindheim, J., Borovkov, V., Hansen, B., Malmberg, S.-Aa, Turrell, B. and Østerhus, S., 2000. Upper layer cooling and freshening in the Norwegian Sea in relation to atmospheric forcing. *Deep-Sea Research I* **47**, 655–680.

Blindheim, J., Toresen, R., and Loeng, H., 2001. Fremtidege klimatiske endringer og betydningen for foskeressursene, *Havets miljø* 73–78.

Box, J.E., 2002. Survey of Greenland instrumental temperature records: 1873–2001. *International Journal of Climatology* **22**, 1829–1847.

Box, J.E., Bromwich, D.H., Bai, L-S, 2004: Greenland ice sheet surface mass balance for 1991–2000: application of Polar MM5 mesoscale model and in-situ data, *J. Geophys. Res.* **109** (**D16**), D16105, DOI: 10.1029/2003JD004451.

Boyer, T., Levitus, S., Garcia, H., Locarnini, R., Stephens, C., and Antonov, J., 2005. Objective analyses of annual, seasonal, and monthly temperature and salinity for the World Ocean on a 0.25° grid. *Int. J. Climatol.*, 931–945, DOI: 10.1002/joc.1173.

Buch, E., 1990. A monograph on the physical oceanography of the Greenland waters. *Greenland Fisheries Research Institute report,* (reissued in 2000 as *Danish Meteorological Institute Scientific Report* **00-12,** Copenhagen), 405 pp.

Buch, E., 2002. Present oceanographic conditions in Greenland waters. *Danish Meteorological Institute Scientific Report* **02-02**, Copenhagen. 39 pp.

Buch, E., Pedersen, S.A., and Ribergaard, M.H., 2004. Ecosystem variability in West Greenland waters. *Journal of Northwest Atlantic Fishery Science* **34**, 13–28.

Cheng, B., 2002. On the modelling of sea ice thermodynamics and air-ice coupling in the Bohai Sea and the Baltic Sea. Ph.D. thesis, Finnish Institute of Marine Research, Helsinki, Finland.

Cuny, J., Rhines, P.B., Niiler, P.P., and Bacon, S., 2002. Labrador Sea boundary currents and the fate of the Irminger Sea water. *Journal of Physical Oceanography* **32**, 627– 647.

Dai, A., Trenberth, K. E., 2002. Estimates of freshwater discharge from continents: Latitudinal and seasonal variations. *J. Hydrometeorol.* **3**, 660-687.

Dickson, R.R., Lazier, J.R.N., Meincke, J., Rhines, P. and Swift, J., 1996. Long-term coordinated changes in the convective activity of the North Atlantic. *Progress in Oceanography* **38**, 241–295.

Dickson, R.R., Meincke, J., Malmberg, S.-Aa., and Lee, A.J., 1988. The "Great Salinity Anomaly" in the northern North Atlantic 1968–1982. *Progress in Oceanography* **20**, 103–151.

Dickson, R.R., Osborn, T.J., Hurrell, J.W., Meincke, J., Blindheim, J., Ådlandsvik, B., Vinje, T., Alekseev, G. and Maslowski, W., 2000. The Arctic Ocean response to the North Atlantic Oscillation. *Journal of Climate* **13**, 2671–2696.

Drinkwater, K.F., Colbourne, E., and Gilbert, D., 2000. Overview of environmental conditions in the Northwest Atlantic in 1999. *NAFO Scientific Council Research Documents* **00/021**.

Hanna, E., and Cappelen, J., 2003. Recent cooling in coastal southern Greenland and relation with the North Atlantic Oscillation. *Geophysical Research Letters* **30**, 1132, doi:10.1029/2002GL015797.

Hurrell, J.W. 1995. Decadal trends in the North Atlantic Oscillation: regional temperatures and precipitation. *Science* **269**, 676–679.

Hurrell, J.W., and van Loon, H., 1997. Decadal variations in climate associated with the North Atlantic Oscillation. *Climate Change* **36**, 301–326.

ICES. 2000. The 1999/2000 ICES annual ocean climate status summary. Prepared by the Working Group on Oceanic Hydrography. Editor: Bill Turrell. (www.ices.dk/status/clim9900/).

ICES. 2001. The 2000/2001 ICES annual ocean climate status summary. Prepared by the Working Group on Oceanic Hydrography. Editors: Bill Turrell and N. Penny Holliday. (www.ices.dk/status/clim0001/).

ICES. 2002. The 2001/2002 ICES annual ocean climate status summary. Prepared by the Working Group on Oceanic Hydrography. Editors: Bill Turrell and N. Penny Holliday. (www.ices.dk/status/clim0102/).

Jacobs, J. D., Radiation climate of Broughton Island. in: Barry, R. G., and J. D. Jacobs (eds.), Energy budget studies in relation to fast-ice breakup processes in Davies Strait: climatological overview. – INSTAAR Occasional Paper, 26, 105–120, Institute of Artic and Alpine Research, University of Colorado, Boulder, CO.

Jakobsen, P.K., Ribergaard, M.H., Quadfasel, D., Schmith, T., and Hughes, C.W., 2003. The near surface circulation in the Northern North Atlantic as inferred from Lagrangian drifters: variability from the mesoscale to interannual. *Journal of Geophysical Research* **108**, C8, 3251, doi:10.1029/2002JC001554.

Jones, J.C., 1990. Patterns of low frequency monthly sea level pressure variability (1899–1986) and associated wave cyclone frequencies. *Journal of Climate* **3**, 1364–1379.

Lilly, J.M., and Rhines, P.B., 2002. Coherent eddies in the Labrador Sea observed from a mooring. *Journal of Physical Oceanography* **32**, 585–598.

Mortensen, J. and Valdimarsson, H., 1999. Thermohaline changes in the Irminger Sea. *ICES CM* **1999/ L:16**.

Nielsen, J.W., Kliem, N., Jespersen, M., and Christiansen, B.M., 2006. Oil drift and fate modelling at Disko Bay. *DMI-Tech. Rep.* **06-06**, Danish Meteorological Institute, Copenhagen, Denmark.

Pedersen, S.A., Ribergaard, M.H., and Simonsen, C.S., 2005. Micro- and mesozooplankton in Southwest Greenland waters in relation to environmental factors. *Journal of Marine Systems* **56**, 85–112, doi:10.1016/j.jmarsys.2004.11.004.

Pickart, R.S., Torres, D.J., and Clarke, R.A., 2002. Hydrography of the Labrador Sea during active convection. *Journal of Physical Oceanography* **32**, 428–457.

Prata, A. J., 1996. A new long-wave formula for estimating downward clear-sky radiation at the surface. *Q. J. R. Meteorol. Soc.* **122**, 1127–1151.

Prater, M.D., 2002. Eddies in the Labrador Sea as observed by profiling RAFOS floats and remote sensing. *Journal of Physical Oceanography* **32**, 411–427.

Ribergaard, M.H., 2004. On the coupling between hydrography and larval transport in the Southwest Greenland waters. Ph.D. thesis. University of Copenhagen. Electronic form: http://ocean.dmi.dk/staff/mhri/Docs/PhD.html

Ribergaard, M.H., 2006. Oceanographic Investigations off West Greenland 2005. *NAFO Scientific Council Documents* **06/001**.

Ribergaard, M.H., and Buch, E., 2004. Oceanographic Investigations off West Greenland 2003. *NAFO Scientific Council Research Documents* **04/001**.

Ribergaard, M.H., Pedersen, S.A., Aadlandsvik, B., and Kliem, N., 2004. Modelling the ocean circulation on the West Greenland shelf with special emphasis on northern shrimp recruitment. *Continental Shelf Research* **24**, 1505–1519, doi:10.1016/j.csr.2004.05.011.

Schmidt, T., and Hansen, C., 2003. Fram Strait ice export during the nineteenth and twentieth centuries reconstructed from a multiyear sea ice index from southwestern Greenland. *Journal of Climate* **16**, 2782–2791.

Shine, K.P., 1984. Parameterization of short wave flux over high albedo surfaces as a function of cloud thickness and surface albedo. *Q. J. R. Meteorol. Soc.* **110**, 747–764.

Valeur, H.H., Hansen, C., Hansen, K.Q., Rasmussen, L., and Thingvad, N., 1997. Physical environment of eastern Davis Strait and northeastern Labrador Sea. *Danish Meteorological Institute Technical Report* **97-09**, Copenhagen.

van Loon, H. and Rogers, J.C., 1978. The seesaw in winter temperatures between Greenland and Northern Europe. Part I: general description. *Monthly Weather Review* **106**, 296–310.

Yang, H., et al. 2005. The DMI-HIRLAM upgrade in June 2004. *DMI-Tech. Rep.* **05-09**, Danish Meteorological Institute, Copenhagen, Denmark.

Previous reports

Previous reports from the Danish Meteorological Institute can be found on:
http://www.dmi.dk/dmi/dmi-publikationer.htm